Clays Clay Miner. (2023) 71:707–721
https://doi.org/10.1007/s42860-023-00264-2

REVIEW

Characterization Study of some Bauxite Deposits in Northern Brazil

Barbara da Rocha Pereira · Morgana Rosset · José Diogo de Oliveria Lima · Keila Palheta Gomes · Denise Crocce Romano Espinosa · Jorge Alberto Soares Tenório

Accepted: 21 November 2023 / Published online: 26 December 2023

Abstract Alumina is produced from bauxite, which contains a mixture of various oxides, such as aluminum (Al), iron (Fe), silicon (Si), and titanium (Ti). Bauxite can also be considered a source of several other valuable metals, such as scandium (Sc), vanadium (V), and gallium (Ga). The composition and mineralogy of alumina determine their economic value, but their characteristics vary by locality. The physicochemical characteristics of bauxites can also be influenced largely by weathering processes, even within the same locality. For this reason, the present study was undertaken with the objective of comparing the characterization data of three bauxite samples collected, which will be referred to as D, E, and F, from the Cruz Alta do Pará plateau in northern Brazil. The samples were solubilized by multi-acid digestion and fusion with lithium metaborate to quantify their metal compositions by inductively coupled plasma optical emission spectrometry (ICP-OES). The mineralogical characterization was conducted by X-ray diffraction (XRD), and the phase changes of minerals in bauxite were detected by thermogravimetric analysis (TGA/DTG). The total organic carbon (TOC) technique was used to quantify the C in the samples, and the moisture content was also measured. Alumina was 30 wt.% on average for all samples, good for producing high-purity alumina by hydrometallurgical processes. The results, however, showed high (~20 at.%) silica concentrations in two samples and ~3 wt.% Fe in one sample, which can pose a challenge in the Bayer process. The X-ray diffraction (XRD) analysis showed that gibbsite (Gbs), kaolinite (Kln), anatase (Ant), and hematite (Hem) were the major mineral phases in these samples. The study showed that the samples from the same mine vary in their metal content, especially with regard to Si, and they, thus, need to be processed selectively to maximize their economic value.

Keywords Alumina · Characterization · Gibbsite · Bauxite

Associate Editor: Yuji Arai

Supplementary Information The online version contains supplementary material available at https://doi.org/10.1007/s42860-023-00264-2.

B. da Rocha Pereira · M. Rosset (✉) · D. C. R. Espinosa · J. A. S. Tenório
LAREX Laboratory of Recycling, Waste Treatment, and Extraction - Chemical Engineering, Department of Polytechnic School of University of São Paulo (USP), São Paulo, Brazil
e-mail: morgana@usp.br

J. D. de Oliveria Lima · K. P. Gomes
MRN Mineração Rio Do Norte, District of Porto de Trombetas, Pará, Brazil

Introduction

Bauxites are considered to be one of the primary economic geological resources for producing

high-purity alumina. Brazil is the third largest supplier of bauxite worldwide (Zhu et al., 2020). Several aluminum (oxyhydr)oxides are known, but only four are found in natural environments. Gibbsite (Gbs) is the most common phase (Dani et al., 2001). Most bauxite deposits were formed during the Mesozoic and Cenozoic eras and and since then have been disturbed by anthropogenic activities. Some deposits have benefited from the enrichment of the aluminum present and eventual reduction of impurities (Mondillo et al., 2022). Two representative groups of bauxites are lateritic bauxites, which account for 90% of the world's mineable bauxite and are found in equatorial regions, and karstic bauxite, which represents ~10% of the world's mineable bauxite and is predominant in various parts of Europe (César et al., 2020; Ruys, 2019b). Bauxite occurs in nature with: (1) carbonate rocks; (2) dolomitic oil shale; (3) an alternative product of dawsonite and aluminohydrocalcite; and (4) minerals that have undergone and continue to undergo weathering processes due to the action of rainfall and rock-leaching processes (Hill, 1980). The lateritic bauxites mainly contain aluminosilicate (Als) type minerals, whereas the karstic bauxites contain smaller quantities of alumina, titanium oxide, and other minerals. Furthermore, rare earth elements in these types of bauxites add economic value (Zhu et al., 2020).

In general, bauxite comprises a heterogeneous mixture of aluminum hydroxides, Kln, silicates, and iron (oxyhydr)oxides. Its composition can vary, from Gbs $Al(OH)_3$, to lateritic bauxite, boehmite (Bhm) γ-AlO(OH), and karstic bauxite, (Abdulvaliyev et al., 2021; Mondillo et al., 2022). In the diasporic (Dsp), karstic bauxite, α-AlO(OH) can be found in specific global locations (Alelweet & Pavia, 2022; Zhang et al., 2018). The composition of bauxite may vary depending on its location, even within the same mine, typically consisting of Kln – $Al_2Si_2O_5(OH)_4$, Hem – Fe_2O_3, goethite (Gth) – FeO(OH), silica (SiO_2), and rutile (Rt) or anatase (Ant) – TiO_2 (Khairul et al., 2019; Ruys, 2019a).

Natural weathering conditions such as pH and temperature directly influence the composition and quantity of aluminum (oxyhydr)oxides (Dani et al., 2001). This is evident in lateritic deposits that are commonly found in extensively weathered tropical and subtropical regions. Bauxites enriched in Fe or Al mainly comprise secondary minerals such as Kln and various iron oxides (Freitas et al., 2018; Muriel et al., 2022).

Karstic bauxite reserves are mainly found in the northern hemisphere. Those in colder climates were formed in the Paleozoic or Mesozoic period, where the climate changes were favorable for the formation of these belts (Mondillo et al., 2021).

Bauxite production in 2021 reached ~1.35 million tons (Zhou et al., 2023) representing an 8% increase over 2020. The countries which exported most bauxite between 2017 and 2020 were Jamaica (62%), Brazil (13%), Guyana (8%), and Australia (6%). Bauxite reserves (Fig. 1) are estimated to be ~55 to 75 billion tons, distributed in Africa, Oceania, South America, and Asia (Yadav et al., 2022).

Bauxite is the main raw material used in the production of alumina through the Bayer process (Habashi, 1997). The material undergoes several processing steps, starting with milling and sieving. Initial pretreatment involves using calcium hydroxide to remove silicon oxides and Kln. Digestion with sodium hydroxide follows to generate sodium aluminate. The resulting solution undergoes a clarification process involving cooling and filtration to remove any remaining impurities (Baudín, 2021; Tabereaux & Peterson, 2014). The treated liquor is transferred to tanks where alumina hydrate crystals are added, leading to the precipitation of aluminum hydroxide. This precipitate undergoes further

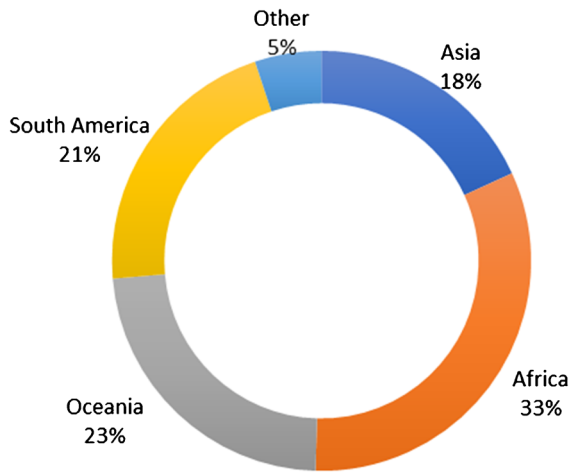

Fig. 1 Bauxite deposits from across the world (Yadav et al., 2022)

https://doi.org/10.1007/s42860-023-00264-2 Published online by Cambridge University Press

washing and calcination in rotary kilns to produce alumina (Agrawal & Dhawan, 2021).

One of the issues encountered during the Bayer process is the presence of silica in bauxite samples, particularly in the form of Kln ($Al_2O_3.2SiO_2.2H_2O$) or reactive silica. This happens because it consumes all of the sodium hydroxide added during the digestion step and it also forms insoluble compounds that hinder the profitability of the Bayer process (Ruys, 2019b). These values are generally considered to be smaller than other bauxite deposits. It is important to note that moisture content of 4–12% can negatively impact the transport of this material (Manjare & Donolikar, 2022).

The presence of this contaminant causes a decrease in performance, leading to moisture absorption and making the alumina particles more susceptible to breakage, resulting in issues with the application of this product. When used in refractories, the quality decreases as it compromises hardness properties, making imports more difficult (Ahmad et al., 2014; Smith & Power, 2021; Wu et al., 2010).

In addition, the formation of deposits in tanks and filters due to the presence of silica causes equipment shutdowns. It is necessary to work with bauxites that have a silica content of <8% in their composition (Tabereaux & Peterson, 2014). When sodium hydroxide is dissolved, silica reacts with alumina and NaOH to form an insoluble sodium aluminum silicate which is then removed from the process as an insoluble component, red mud (RM). This reaction leads to the loss of NaOH. If a bauxite with high silica content is treated using the Bayer process, typically the mud is recovered and undergoes an expensive process to recover the lost aluminum and NaOH (Ostap, 1986).

One of the most common issues in the industry is the dissolution of silica. Silica solubility can be found in the form of orthosilicic acid, H_4SiO_4, at a pH of <7. These monomers bind together and form polymeric silicic acid, which can be identified in the formation of a colloid that contains trapped liquids within, resulting in gelation (Botelho et al., 2021). At the end of the Bayer process, red mud rejects are generated, which contain high concentrations of Al, Fe, and Si. High concentrations of Fe, as well as silica, cause issues regarding the purity of the alumina produced in the final stage of the Bayer process (Jiang et al., 2021). Approximately 1.0–1.5 tons of RM waste is generated during the Bayer process (Clark et al., 2015). The chemical composition of RM consists of all the elements that were not extracted at the end of the Bayer process. The waste is rich in Fe, Ti, silica, and may contain smaller amounts of other compounds such as V, Ga, phosphorus, manganese (Mn), magnesium (Mg), zinc (Zi), chromium (Cr), niobium (Ni), and others (Luo et al., 2014). The red mud is a highly alkaline waste with a pH of 13. It is stored in dam systems which can lead to accidents. Storing it in dams requires manpower and financial resources and occupies land that loses its value as a result. Pollution incidents have occurred in China, India, and Hungary, among others (Xue et al., 2019).

Recovering elements of interest such as Al and rare earths through hydrometallurgical processes becomes challenging due to the presence of Fe and Si in their composition. When RM is recycled, the aim is also to locate materials with added value, thereby reducing the use of natural resources and extending the life of the waste lagoons (Agrawal & Dhawan, 2021). About 1.0–1.5 tons of RM waste is produced per ton of alumina produced. This range depends on the quality of the bauxite (Castaldi et al., 2008, 2011). Therefore, mineralogical and elemental characterizations of bauxite are essential for mining.

While these studies provided valuable information about Kln, $Al(OH)_x$ polymorphs, and nordstrandite in bauxites from India and Brazil, the results did not use the critical information about detailed Al mineralogy and the Si content that are critical in the Bayer process. The objective of the present study, therefore, was to characterize in detail the bauxites of the Cruz Alta do Pará plateau in northern Brazil, especially with respect to their metals composition, to help the aluminum industry there by improving the efficiency of the extraction process.

Materials and Methods

Three bauxite samples from the Cruz Alta do Pará plateau were supplied by the mining company MRN (Mineração Rio do Norte), located in Pará, Brazil. The mineralogical analysis was carried out at the LAREX (Recycling, Waste Treatment, and Extraction Laboratory) at the University of São Paulo, Brazil. Samples D, E, and F were obtained from excavated sites (Fig. 2) and exhibited distinctly different characteristics.

https://doi.org/10.1007/s42860-023-00264-2 Published online by Cambridge University Press

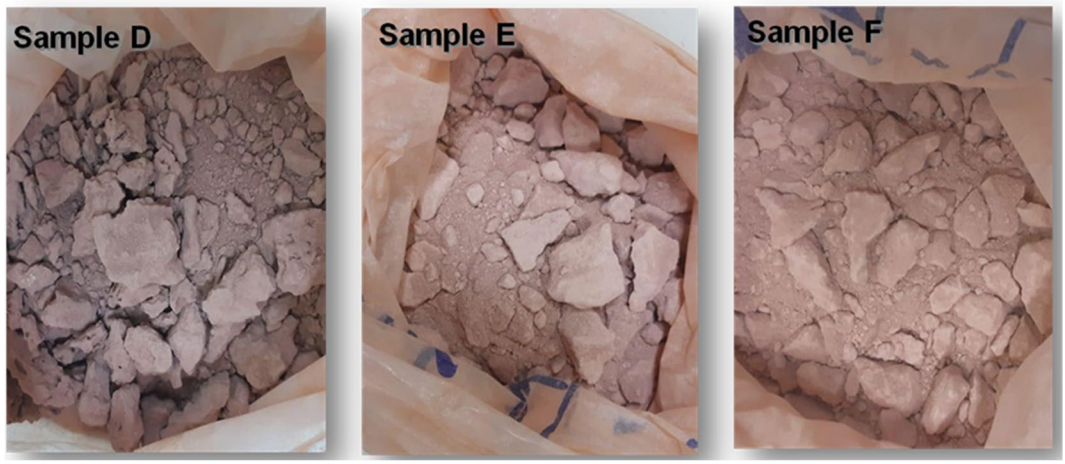

Fig. 2 Bauxite samples D, E, and F from the Cruz Alta do Pará plateau in northern Brazil

Each sample underwent homogenization, quartering, and subsequent storage. Particle-size analysis was conducted, and all samples were ground in an agate mill until they reached a particle size of <0.212 mm. X-ray diffraction (XRD), moisture content, loss on ignition, total organic carbon (TOC), and thermogravimetric analysis (TGA/DTA) were performed to characterize the samples. To quantify the metals contained in the samples, two systems were employed: multi-acid microwave digestion and lithium metaborate fusion digestion.

Particle-size Analysis

Particle-size analysis involved the use of ten Tyler series sieves from the brands Bronzinox and Granutest with mesh sizes of 9.50 mm (3/8'' mesh), 4.699 mm (4 mesh), 2.362 mm (8 mesh), 1.44 mm (14 mesh). 1.00 mm (18 mesh), 0.500 mm (35 mesh), and 0.150 mm (100 mesh). The sieves were placed in an AB Bronzinox – model AG5G 17 automatic shaker (Bronzinox Co., São Paulo, Brazil) for 15 min. After completing the granulometric analysis stage, the samples were divided into quarters and ground in an agate mill, model Marconi MS950 (São Paulo, Brazil), until reaching a particle size of <0.212 mm.

Moisture Content, Loss on Ignition, and Total Organic Carbon Analyzer

Moisture content was analyzed using a GEHAKA model IV2000 infrared moisture analyzer (Goiâna, Brazil). About 3 g of each bauxite sample was utilized in the experiments, with all tests conducted on previously ground samples with a granulometry of 0.212 mm. Furthermore, the tests were conducted twice for accuracy and validity.The samples were placed in porcelain crucibles and subjected to a muffle furnace (Jung, model LF00812, Blumenal, Santa Catarina, Brazil) with a heating rate of 10°C min^{-1} up to 1200°C, where they remained for 2 h. The percent loss on ignition (LoI) was determined by Eq. 1, where $M1$ represents the initial mass and $M2$ represents the remaining mass at the end of the LoI test (Liu et al., 2023; Nguyen et al., 2023).

$$LoI(\%) = \left(\frac{M1 - M2}{M1}\right) * 100 \quad (1)$$

To determine the total organic carbon in the solid samples, a Shimadzu total organic carbon analyzer model SSM-5000A (Shimadzu Brazil, São Paulo, Brazil) was utilized. Approximately 30 mg of each sample was used, with the first analysis conducted at

https://doi.org/10.1007/s42860-023-00264-2 Published online by Cambridge University Press

900°C to determine the total carbon through combustion. 30 mg of the sample and 1 mL of sulfuric acid were added to the equipment to evaluate the inorganic carbon at 200°C. After completion of the test, the total organic carbon was calculated as the difference between the total and inorganic carbon.

X-ray Diffraction (XRD)

The mineralogical compositions of the three bauxite samples was measured using a Rigaku model MiniFlex 300 X-ray diffractometer (Rigaku Corporation, Tokyo, Japan) with CuKα radiation (λ = 1.5418 Å). Rietveld refinement was employed, ranging from 5 to 80°2θ with a 0.02°2θ step size, in 'continuous' mode at a speed of 4°2θ min^{-1}. The XRD pattern was evaluated, and the phases present were quantified using the PDXL Studio database (Rigaku Corporation, Tokyo, Japan).

Thermogravimetric Analysis (TGA/DTA)

The thermogravimetric analysis (TGA) was performed by means of a thermobalance coupled with differential thermal analysis using a Jupiter STA449 F1 instrument (Netzsch, São Paulo, Brazil). Initially, 50 mg of the bauxite sample was placed in an Al_2O_3 crucible and heated from 25 to 1450°C, with a heating rate of 10°C min^{-1}. The analysis was conducted in an argon atmosphere with a flow rate of 25 mL min^{-1}, and the samples remained at the maximum temperature for 30 min.

Multi-acid Microwave Digestion

Two methodologies were utilized to quantify the chemical composition of the samples. First, acid digestion was performed using a CEM model MARS6 microwave sample digester (CEM Corporation, Matthews, North Carolina, USA). Approximately 0.25 g of each of the three bauxite samples was used. The decomposition of the original matrix required three steps. In the first step, 6.5 mL of H_3PO_4 (Synth, São Paulo, Brazil—P.A. 85%) and 3.5 mL of H_2SO_4 (Synth, São Paulo, Brazil—P.A. 98%) were added, and the samples were heated at 240°C for 15 min. In the second step, 1 mL of HCl (Synth, São Paulo, Brazil—P.A. 38%), 1 mL of HNO_3 (Synth, São Paulo, Brazil—P.A. 65%), and 1 mL of HF (Neon, São Paulo, Brazil—P.A. 48%) were added, and the samples were maintained at 200°C for 15 min. In the last step, 0.4 g of boric acid (Synth, São Paulo, Brazil) and 8 mL of water were added, and the samples were left in the device for 15 min to neutralize the presence of hydrofluoric acid.

Lithium Metaborate Fusion

Lithium metaborate fusion was used to quantify the chemical composition associated with rocks and refractory minerals, such as aluminum in Gbs in the three samples. Samples were prepared according to published methods (Abedini et al., 2022a; Pang et al., 2023). Approximately 3 g of each sample was combined with 6 g of lithium metaborate salt $LiBO_2$ (Synth, São Paulo, Brazil) in super-pure graphite crucibles. The crucibles were then heated in a Jung muffle furnace model LF 00812 (Jung, Blumental, Santa Catarina, Brazil) with a temperature ramp at the rate of 10ºC min^{-1}, starting from 100ºC to 1050°C for 2 h. Afterward, the crucibles, still hot at ~900°C, were removed from the muffle furnace and their contents were poured into a beaker containing a 10% HCl solution. The samples were then stirred on plates for 30 min, filtered through a 2 µm Whatman filter (Química moderna, São Paulo, Brazil), and stored for further analysis.

Optical Emission Spectrometry with Plasma-ICP-OES

Two calibration curves were prepared to analyze the digestion liquors using a coupled plasma optical emission spectrometer (ICP-OES) model 710 series (Agilent, Santa Clara, California, USA). The first curve utilized the multi-elemental standard GV2 with a concentration of 100 mg/L (SpecSol, São Paulo, Brazil) in 65% HNO_3. The elements to be analyzed were Al, Ca, Mg, K, Na, and Fe, with 1 to 10 mg/L concentrations. The second curve employed a mono-elemental silicon standard with a concentration of 1000 mg/L (SpecSol, São Paulo, Brazil) and concentrations of 1, 2, 4, 6, 8, and 10 mg/L. 3% HNO_3 (P.A. 65%) acid was used to prepare standards diluted 5-,10-,100-, and 1000-fold. Wavelengths that were least affected by neighboring peaks were selected for the respective elements: Al (396 nm), Ca (396 nm),

https://doi.org/10.1007/s42860-023-00264-2 Published online by Cambridge University Press

Fig. 3 Bauxite sample during grain-size distribution tests

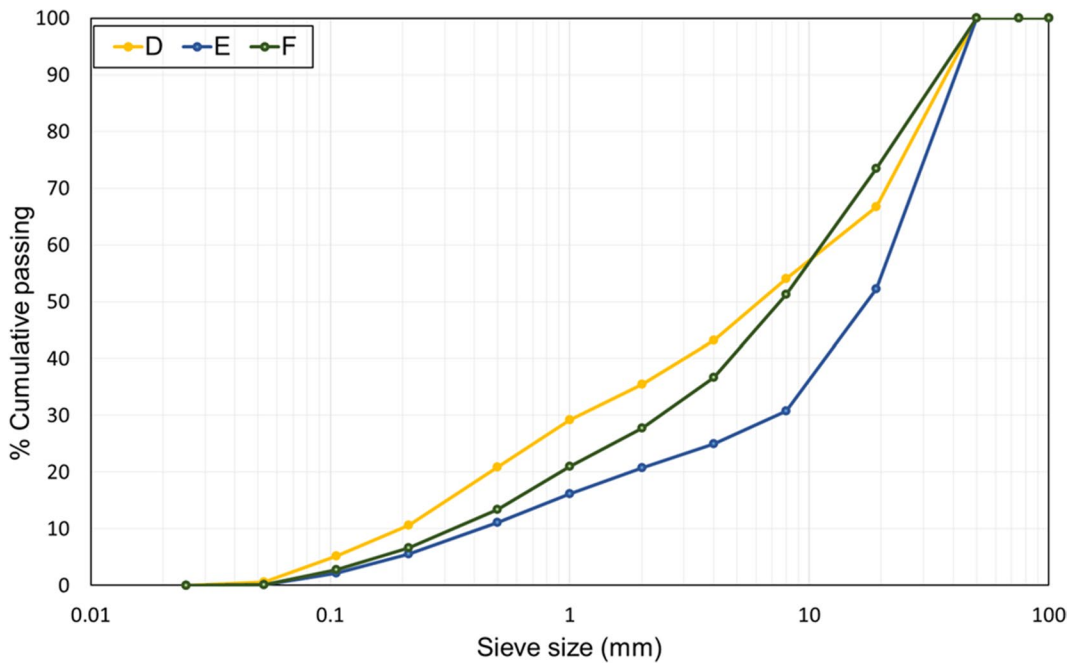

Fig. 4 Particle-size distribution of the bauxite samples D, E, and F

Fe (238 nm), K (766 nm), Mg (279 nm), Ti (336 nm), Na (589 nm), and Si (251 nm).

Results and Discussion

Particle-size Analysis

Examples of fractionated samples in each sieve are shown in Fig. 3. The particle-size distribution for sample D (Fig. 4) revealed a D10 (effective diameter) value of 0.2 mm, indicating that 10% of the particles were of a diameter of 0.2 mm, considered to be a medium size. The values D50 and D90 were 6 mm and 37 mm, respectively. Once again, fine particles predominate in this sample. When the data for sample E were examined (Fig. 4), D10 was 0.4 mm, D50 was 18 mm, and D90 was 40 mm. This indicates that only 10% of the sample consists of particles with sizes > 40 mm, highlighting a predominance of

https://doi.org/10.1007/s42860-023-00264-2 Published online by Cambridge University Press

smaller-sized particles. In contrast, sample F (Fig. 4) exhibited the following values: 0.3 mm, 7.5 mm, and 35 mm for D10, D50, and D90, respectively. In this case, undersized particles make up the majority (50%) of the sample with only 10% at quantitative values (10% cumulative passing of samples). One concludes, therefore, that sample D contains particles with larger sizes than samples E and F, but all samples are predominantly composed of fine particles.

The Rosin-Rammler-Bennet studies (RRB) indicated that the grinding time affects particle characteristics, necessitating adjustments to the processing parameters (Zhang et al., 2014). On the other hand, Wrebec's mathematical model evaluates particles of <50 µm, resulting directly from crushing (Mohan et al., 2014). When the grinding time is increased for particles ranging from 0–3 to 3–10 µm, no variation in the mechanical fraction and particle-size values was observed. Increasing the grinding time for particles within this range therefore, only leads to unnecessary energy consumption, as it does not affect the mechanical fraction (Liu et al., 2016; Mohan et al., 2014).

Several mathematical models can be used to determine the particle-size phases D10, D50, and D90 from grinding, such as the RRB (Eq. 2) and Gates-Gaudin-Schuhman (GGS) (Eq. 3) models. *k, m, n,* and *D'* are the parameters to be adjusted to fit the experimental data (Wu et al., 2004). Of these two models, the RRB function performs better, particularly when a ball mill is used for grinding the samples. Combining multiple functions, however, is generally more effective than relying solely on a single mathematical model (Chu et al., 2019). So, consider: X = mass fraction of material finer than the sieve opening (kg/kg total); D' = parameter representing the average particle size (µm); n = parameter representing dispersion (dimensionless); D = the opening of the sieve of order n (m); k = parameter representing the average particle size (µm); m = parameter representing dispersion (dimensionless), also called Schuhmann's derivative.

$$X = 1 - \exp\left[-\left(\frac{D}{D\prime}\right)^{n}\right] \tag{2}$$

$$X = \left(\frac{D}{k}\right)^{m} \tag{3}$$

Table 1 Equations for the mathematical models

Mathematical models	Parameters	Samples D	E	F
	m	0.4627	0.5445	0.5946
GGS	k	0.7997	0.0968	0.1055
	R^2	0.9217	0.9340	0.9538
	n	0.5499	0.5996	0.6933
RRB	D'	0.0008	0.0003	0.0008
	R^2	0.9539	0.9499	0.9774

Mathematical models are essential to obtain the statistical parameters used in industrial processes. The plots using the mathematical models of granulometric distribution RRB and GGS for bauxites D, E, and F are available in the supplementary material (Figs S1, S2, and S3). The coefficient of determination (R^2) indicated that the RRB model (Table 1) provided a better fit. The value of m was < 1 in all samples (Table 1), thus showing that the material does not have a uniform particle size.

The Fanrenwald model proposes a correlation between the reduction rate of residue on the sieve and the particle size, highlighting the relationship between grinding speed and the accumulated percentage on the sieve after a certain grinding period x (Chen et al., 2020). These two factors are directly proportional during grinding (Liu et al., 2016). Grinding efficiency is correlated with particle size, meaning that as particle size decreases, grinding efficiency also decreases (Liu et al., 2016; Wang et al., 2021). When analyzing the D10, D50, and D90 percentages, the accumulated volumetric distribution and width were evaluated, facilitating the manipulation of the samples. The grinding time and the kinetic energy provided during this process are

Table 2 Moisture content and loss on ignition values for the three samples

Bauxite samples	Moisture (%)	Loss on ignition (%)
D	0.5	24.4
E	0.9	20.4
F	0.8	19.6

https://doi.org/10.1007/s42860-023-00264-2 Published online by Cambridge University Press

associated with the particle-size distribution values (Fabre et al., 2020).

Moisture Content, Loss on Ignition, and Total Organic Carbon Analyzer

The samples exhibited relatively low moisture content levels (Table 2), with values < 1.0%. Comparing the samples revealed that sample D had a smaller moisture content (0.5%) than samples E and F (0.9 and 0.8, respectively). These values are generally considered to be smaller than other bauxite deposits. It is important to note that moisture content of 4–12% can negatively impact the transport of this material (Manjare & Donolikar, 2022).

The mass loss on ignition in this test is related to the loss of structural water (Table 2). In the studies by Liu and Poon (2016), the LoI in rejected red mud (generated after the clarification stage in the Bayer Process) originating from China was 8.14%. In the research of Gräfe et al. (2011), after several analyses of red mud samples, the values of LoI varied from 4.4 to 14%. In rejected red mud originating from Brazil, the LoI varied with temperature; at 900 and 1100°C the LoI was 14.5 and 14.8%, respectively (Botelho et al., 2021). In the studies by Botelho et al. (2020), the values for inorganic carbon and total carbon were 0.32% and 0.6%, respectively, so organic carbon remained at ~0.28%. Power and Loh (2010) evaluated the organic carbon values in bauxite from Guinea, Brazil, and Suriname, where the percentages were 0.25%, 0.18%, and 0.47%, respectively.

The total organic carbon was measured in the organic and inorganic matter in the sample and none was found (Banerjee et al., 2023). The presence of organic matter would lead to an increase in the production costs of the alumina because the organic matter is considered a contaminant in the process. All lateritic bauxites contain a certain amount of organic carbon compounds, some of which are solubilized during the digestion process. As a result, organic compounds accumulate in the process liquor (Castaldi et al., 2008; Power & Loh, 2010; Santini, 2015). An assessment of the impact of these compounds on production costs revealed that the annual expenses

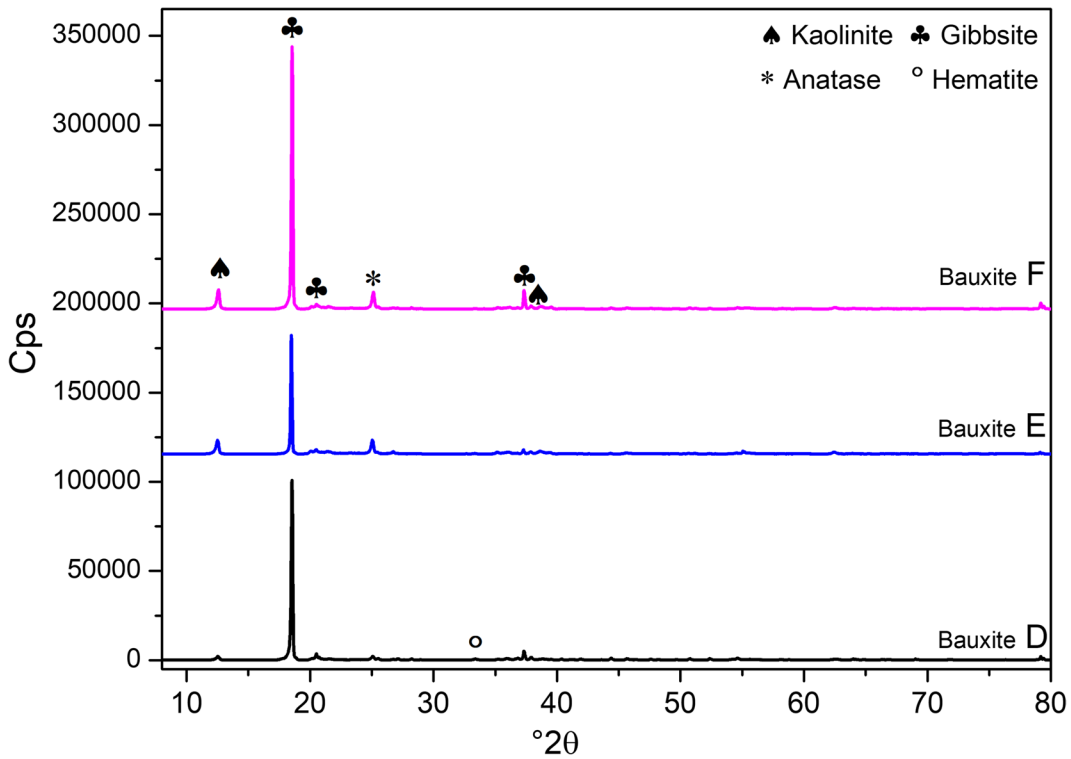

Fig. 5 XRD patterns of the bauxite samples

https://doi.org/10.1007/s42860-023-00264-2 Published online by Cambridge University Press

for the Australian alumina industry alone exceeded AUD$ 500 million where organic products were concerned (Power et al., 2012). The Brazilian bauxites do not consume more reagent during the digestion stage.

X-ray Diffraction (XRD)

The mineralogical composition of the three bauxite samples was determined using XRD (Fig. 5), and the phases were calculated using the Rietveld method (Castaldi et al., 2008; Santini, 2015). The Rietveld method identified Gbs as the predominant phase in all samples (Table 3), comprising ~50–80% of the composition. Smaller amounts of Kln (~20–30%), Ant (3–6%), and Hem (5%) were also present. This is in accordance with the literature (César et al., 2020; Santini, 2015).

Sample E contained most Gbs (75%), which is desirable due to its greater potential to yield aluminum (Table 3). However, a large (20%) Kln content in this sample poses a challenge during the Bayer Process. The reactive silica found in Kln consumes a significant amount of calcium hydroxide and subsequently affects the extraction of aluminum hydroxide. Reactive silica values (SiO_2) in the the lithium metaborate digestion data were 4.35, 3.16, and 3.23 wt.% in samples D, E, and F, respectively. Bauxite compositions containing <8% reactive silica are noteworthy and recommended in order to minimize excessive reagent consumption (Tabereaux & Peterson, 2014).

The Kln content of sample F is large at 26.29 wt.%, indicating the need to explore alternative methods to the Bayer process for recovering usable Al and removing impurities from this sample. In addition, sample D exhibited the greatest iron oxide content, ~5%. In comparison, sample E showed the removal of 3.9% titanium oxide during the Bayer process, resulting in the generated tailings known as red mud (Ahmad et al., 2014). Another factor to consider is the presence of amorphous content, which may not be quantified accurately by the analytical techniques used in the present study. As a result, the calculated amount of crystalline content may be overestimated (Alelweet & Pavia, 2022).

Rietveld quantitative analysis of bauxite from a mine in Russia revealed Gbs 55.2%, Kln 10%, titanium oxide 4.9%, and iron oxide 4.9% (Abdulvaliyev et al., 2021). The XRD patterns of bauxite provided by Paragominas Mining (Pará, Brazil) revealed predominantly Gbs, with lesser amounts of Kln, Hem, Gt, and Ant (Dodoo et al., 2022). A mine in Ghana produced samples with 10 wt.% SiO_2, 50 wt.% Gbs, and 3.15 wt.% iron oxide, as well as ~2 wt.% oxides of Mg, Na, Ca, and K combined (Melo et al., 2020).

XRD patterns of samples from mines in central and northern Saudi Arabia revealed high crystallinity, with intense peaks from Gbs, Kln, and Bhm. Interestingly, those bauxites consisted of >50 wt.% boehmite and Gbs, with only 15 wt.% Kln along with other minor components of Ant, rutile (Rt), calcite (Cal), and Qz making up ~7 wt.% each (Alelweet & Pavia, 2022). Bauxite from various provinces of China have a mineralogical composition of silicon oxide plus diaspore of ~58 wt.%, while iron oxide and titanium comprise 24.23 and 3.12 wt.%, respectively (Wu et al., 2022b).

Table 3 Rietveld profile analysis

Phases	Samples		
	D	E	F
Gbs	74.3	75	67.5
Hem	5	1.1	0.23
Kln	18.1	20	26.2
Ant	2.5	3.9	6.1

Thermogravimetric Analysis (TGA)

Thermogravimetric analysis (TGA/DTGA) (Fig. 6) revealed in the first stage, spanning 100 to 360°C, significant mass losses from samples D, E, and F, measuring 16.88, 11.27, and 8.50 wt.%, respectively. An intense endothermic peak at 300°C indicated the transformation of the Gbs into the first metastable alumina phase (χ-Al2O3). At 300°C, Gbs undergoes dehydroxylation and converts into boehmite, as described by the decomposition Eq. 4 (Zhang et al., 2019).

$$Al(OH)_3 \rightarrow AlOOH + H_2O \quad (4)$$

In the second stage, from 360 to 600°C, the mass losses were 6.79 wt.% for sample D, 6.74 wt.% for sample E, and 9.81 wt.% for sample F. Another endothermic event at ~515°C signified the formation of a

https://doi.org/10.1007/s42860-023-00264-2 Published online by Cambridge University Press

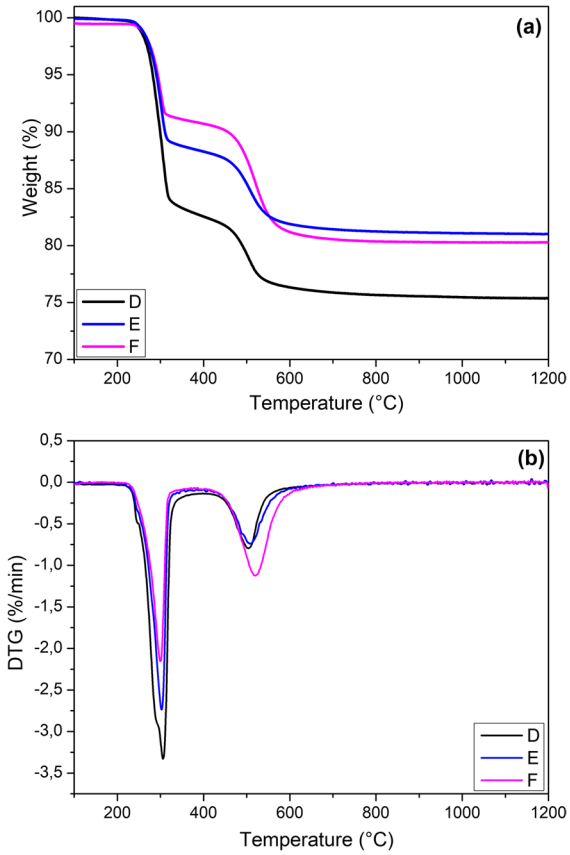

Fig. 6 Thermogravimetric profiles of the bauxite: **a** TG and **b** DTG

second metastable phase of alumina (κ-Al_2O_3) (Alelweet & Pavia, 2022; Li et al., 2020a). With the loss of the hydroxyl groups from the samples containing Kln, the formation of amorphous metakaolinite occurred from 400 to 650°C (Lagauche et al., 2017). In the third stage, ranging from 600 to 1200°C, the mass losses for D, E, and F were 1.17, 0.88, and 0.91 wt.%, respectively. During this stage, as the temperature increased from 900 to 1200°C, the amorphous alumina phases (ϒ-Al_2O_3) underwent regrouping to form the corundum phase α-Al_2O_3 (Arogundade et al., 2021; Kyriakogona et al., 2017). This mass loss aligns with the LoI observed in the chemical analysis, attributed primarily to the release of hydroxyl groups present in the minerals. Relating the TGA test to the LoI test is possible.

Multi-acid Microwave Digestion and Lithium Metaborate Fusion

The significant elements analyzed, including Fe, Al, Si, and Ti, were subjected to microwave and fusion digestion methods (Table 4). Oxides were calculated based on the amounts of the individual elements obtained in the analyses.

The results revealed that aluminum oxide was the most abundant compound in the samples, followed by silicon oxide, with smaller concentrations of titanium and iron oxide. A comparison between the two digestion methodologies showed variations in the element contents, indicating differences between the analytical techniques used to determine the elements present. Microwave digestion was the more sensitive method in terms of iron and titanium oxides, suggesting that metaborate fusion is not a consistent technique for elements present in smaller quantities (Giels et al., 2022).

Based on the assays, atomic absorption spectrometry using a microwave-based opening methodology was deemed the most suitable technique for chemical analysis, specifically for samples D, E, and F. The

Table 4 Data obtained from the chemical analyses in the lithium metaborate and multi-acid digestions in ICP-OES

Elements analyzed by ICP-OES lithium borate fusion digestion (%)													
Samples	Al	Al_2O_3	Si	SiO_2	Fe	Fe_2O_3	Ti	TiO_2	Ca	K	Mg	Na	
D	17.7	34.0	2.1	4.5	2.7	3.9	0.1	0.1	0.0	0.7	0.1	0.7	-
E	14.2	30.0	9.2	19.6	0.9	1.4	0.0	0.1	0.0	0.7	0.1	0.1	-
F	18.7	36.0	8.5	18.1	1.0	1.4	0.1	0.1	0.0	0.8	0.1	0.7	-
Elements analyzed in ICP-OES multi-acid digestion													
Samples	Al	Al_2O_3	Si	SiO_2	Fe	Fe_2O_3	Ti	TiO_2	Ca	K	Mg	Na	V
D	22.5	44.0	10.1	22.0	3.8	5.4	1.2	2.0	3.1	-	0.0	3.8	-
E	18.4	36.0	15.9	35.0	1.6	2.2	0.9	1.5	3.0	-	0.0	3.5	-
F	19.8	38.0	12.3	28.0	1.3	1.9	1.1	1.8	3.1	-	0.0	3.7	-

https://doi.org/10.1007/s42860-023-00264-2 Published online by Cambridge University Press

multi-acid digestion in HNO_3, HCl, H_2SO_4, and HF solutions was an effective procedure for evaluating many elements in various mineral species. The addition of phosphoric and sulfuric acid facilitated the extraction of aluminum, while nitric acid reacted with other metals present, such as titanium, magnesium, calcium, sodium, and potassium. Hydrofluoric acid reacted primarily with the silica content in the samples (Dillinger et al., 2020).

Silica, when in the form of Kln, poses a problem in the Bayer process as it reacts with NaOH during bauxite digestion, forming insoluble compounds that reduce the profitability of the process. In contrast, when silica is in the form of quartz, it exhibits inert behavior and does not significantly impact the consumption of NaOH, referred to as non-reactive silica. It is crucial to work with bauxites containing <8% reactive silica in their composition to mitigate these issues (Tabereaux & Peterson, 2014).

Approximately 80–90% of calcium hydroxide is lost during the process, posing a significant issue. Consequently, utilizing bauxites with <8 wt.% reactive silica content is essential to mitigate this problem (Ahmad et al., 2014; Smith & Power, 2021; Wu et al., 2010).

Iron oxides in bauxite are also problematic in alumina production. Although the samples used in the experiments had values of <5 wt.% Fe_2O_3, worldwide samples, especially from China and Iran, tend to have larger iron oxide contents. The iron oxide impurities are removed during the clarification process, resulting in the red mud.

Titanium oxides are generally non-reactive but can hinder precipitation and reduce reaction yields when present as boehmite. Although the samples showed titanium oxide values of <1 wt.%, global bauxites often have values of >5 wt.%.

Comparing the composition of bauxites from various locations worldwide (Table 5), Australia, China, and Saudi Arabia typically have aluminum oxide values of ~50 wt.%. In comparison, the bauxites from Porto de Trombetas exhibit 40 wt.% Al_2O_3. Regarding the iron oxide content, bauxites from mines in Iran, China, and Greece have values ranging from 20 to 30 wt.% of Fe_2O_3, while Russia and Saudi Arabia show values of 5 wt.%. The samples obtained in the experiments align with these findings, with iron oxide amounts of 4 wt.%. Titanium oxide values in global bauxites are usually >5 wt.%, whereas the samples analyzed in this study had <1 wt.%. Silicon oxide

Table 5 Oxide percentages in bauxites from around the world

Location	China	Iran	Greece PSI-3	Northwest Iran	Australia	China		Russia	China	Saudi Arabia
CaO	0.41	1.22	<0.01	-	-	0.065	0.026	-	-	1.15
Fe_2O_3	9.23	25.40	29.04	32.90	9.46	1.9	14.66	5.56	2.5	4.00
Al_2O_3	54.50	46.89	52.69	36.10	51.28	56.75	61.42	49.26	50.8	52.53
Na_2O	0.007	-	0.01	-	0.02	0.12	0.051	-	0.1	0.19
MgO	0.11	-	0.65	1.0	0.06	0.34	1.3	-	2.47	0.13
K_2O	0.30	0.09	<0.01	0.1	-	0.17	0.03	-	-	0.06
SiO2	17.06	12.05	0.86	15.00	9.58	22.96	7.48	24.18	29.2	14.85
TiO_2	2.69	2.10	4.15	5.4	3.11	2.93	2.18	2.94	1.9	4.78
LOI	15.69	12.25	12.59	9.4	25.15	14.2	12.93	16.02	14.50	-
Reference	(Li et al., 2022)	(Behmadi et al., 2022)	(Mondillo et al., 2022)	(Abedini et al., 2022a, 2022b)	(Wu et al., 2022a)	(Zhang et al., 2022)		(Valeev et al., 2021)	(Li et al., 2020b)	(Alelweet & Pavia, 2022)

https://doi.org/10.1007/s42860-023-00264-2 Published online by Cambridge University Press

measurements in bauxites worldwide range from 20 to 26 wt.%, similar to the values obtained in the chemical analyses of the three samples. Dealing with the silicon oxide content is crucial as it represents one of the main challenges in the Bayer process.

Discussion of alumina production in bauxites from northern Brazil

Many published studies discuss various types of bauxite. However, a comprehensive characterization of bauxite has never been carried out, which highlights the need to design a process to overcome the challenges in understanding this material. In addition, exploring new approaches for the recovery of elements of interest is important. A comprehensive description of bauxite is required to develop hydrometallurgical processes for the recovery of elements of interest, such as rare earths, or to develop new routes for aluminum production. Sample D contains 10 wt.% silica, which is considered to be less than in samples from China, Russia, and Iran, where silica values reach ~20 wt.%.

A proposed solution to eliminate silica and prevent interference in the Bayer process and the development of other hydrometallurgical routes is calcination, as kaolinite transforms into metakaolinite at ~600°C, leading to the removal of the silicon (Alelweet & Pavia, 2022).

The acid leaching of bauxites involves using oxalic, sulfuric, and hydrochloric acids. Oxalic acid, due to its acidity and ability to form complexes with iron, can extract iron at levels ranging from 34 to 85%, producing iron oxalate (Arogundade et al., 2021). Sulfuric acid can also effectively remove significant amounts of iron, typically from 47 to 98%, from bauxite and red mud samples (Kyriakogona et al., 2017). Hydrochloric acid leaching can achieve a 90% iron removal from the leach liquor by forming $FeCl_3$. In bauxites primarily composed of boehmite, the aluminum removal rate is ~10% (Alelweet & Pavia, 2022). Leaching is commonly employed for alumina recovery and proves more efficient than alkaline methods. Certain acids can reduce silica solubilization and remove other elements such as iron (Zhu et al., 2020). The high concentration of acid during leaching generates the dissolution of the silica present in the sample, thus generating the polymerization of the silica gel, with which the extraction efficiency is reduced. When silica undergoes the leaching process with sulfuric acid, the monomers unite to form polysilicic acid and, later, a colloid. This formation is related to the ionic forces present in the solution, where molecular interactions are altered when the acidity of the leaching is high (Zhou et al., 2021). It is proposed that silica gel formation be avoided by using sulfuric acid with hydrogen peroxide for oxidative leaching to oxidize the silicon ions dissolved in the solution, thus avoiding the polymerization reaction (Botelho et al., 2021). For samples E and F, which have silica concentrations of >20 wt.%, additional processes need to be applied in order to use them. For other impurities, all samples have iron concentrations of <3 wt.%, while other bauxites mentioned in the literature have concentrations >20 wt.%. Improving the quality of purification processes often presents challenges when it comes to iron.

Conclusions

The aim of the present study was to analyze bauxite samples and compare them with other samples from around the world. A comprehensive characterization was conducted on bauxite samples from northern Brazil. The Brazilian bauxite exhibits lower concentrations of silicon and iron in comparison to bauxite samples from other regions of the world, such as Russia and China. In this study, multiple characterizations were employed to enhance the technical understanding of Brazilian bauxites. Indeed, enhancing the technical understanding of any sample, particularly bauxites, aids in identifying their potential applications and determining the need for pre-treatment or other processes prior to alumina production, for instance. The results showed that the samples could be used in hydrometallurgical processes, such as acid leaching, to obtain the recovery and production of alumina. The silicon concentration is one of the main challenges encountered due to silica gel formation. Thus, exploring leaching routes that do not excessively consume the acids used in the process is important.

Acknowledgements The authors are grateful for the financial support of Mineradora Rio do Norte (MRN) and the Brazilian Company of Research and Industrial Innovation (EMBRAPII-TECNOGREEN 41829). Grant 2019/11866-5 São Paulo Research Foundation (FAPESP).

Declarations

Conflict of Interest The authors declare that they have no conflicts of interest.

References

Abdulvaliyev, R. A., Dyussenova, S. B., Manapova, A. I., Akcil, A., & Beisenbiyeva, U. Z. (2021). Modification of the phase composition of low-grade gibbsite-kaolinite bauxites. *Kompleksnoe Ispol'zovanie Mineral'nogo Syr'â/complex Use of Mineral Resources/mineraldik Shikisattardy Keshendi Paidalanu, 317*, 94–102.

Abedini, A., Mongelli, G., & Khosravi, M. (2022a). Geochemistry of the early Jurassic Soleiman Kandi karst bauxite deposit, Irano-Himalayan belt, NW Iran: Constraints on bauxite genesis and the distribution of critical raw materials. *Journal of Geochemical Exploration, 241*, 107056.

Abedini, A., Khosravi, M., & Mongelli, G. (2022b). The middle Permian pyrophyllite-rich ferruginous bauxite, northwestern Iran, Irano-Himalayan karst belt: Constraints on elemental fractionation and provenance. *Journal of Geochemical Exploration, 233*, 106905.

Agrawal, S., & Dhawan, N. (2021). Evaluation of microwave acid baking on Indian red mud sample. *Minerals Engineering, 160*, 106686.

Ahmad, I., Hartge, E. U., Werther, J., & Wischnewski, R. (2014). Bauxite washing for the removal of clay. *International Journal of Minerals, Metallurgy and Materials, 21*, 1045–1051.

Alelweet, O., & Pavia, S. (2022). Pozzolanic and hydraulic activity of bauxite for binder production. *Journal of Building Engineering, 51*, 104186.

Arogundade, A. I., Megat-yusoff, P. S. M., Ahmad, F., Bhat, A. H., & Afolabi, L. O. (2021). Modification of bauxite residue with oxalic acid for improved performance in intumescent coatings. *Journal of Materials Research and Technology, 12*, 679–687.

Banerjee, P.K., Mankar, A.U., & Kumar, V. (2023) *Beneficiation of bauxite ores*. P. in: *Mineral Processing: Beneficiation Operations and Process Optimization through Modeling*. INC, 117–166 pp

Baudín, C. (2021) Alumina, Structure and Properties. Pp. 25–46 in: *Encyclopedia of Materials: Technical Ceramics and Glasses*. Elsevier. https://doi.org/10.1016/B978-0-12-818542-1.00028-X

Behmadi, R., Mokhtarian, M., Ghadrian, K., Davoodi, A., & Hosseinpour, S. (2022). Development of a low-cost activated mesoporous bauxite for the reclamation of used transformer oil. *Separation and Purification Technology, 280*, 119826.

Botelho, A. B. J., Espinosa, D. C. R., & Tenório, J. A. S. (2020). Characterization of Bauxite Residue from a Press Filter System: Comparative Study and Challenges for Scandium Extraction. *Mining, Metallurgy & Exploration, 38*, 16.

Botelho, A. B. J., Crocce, D. E., & Tenório, J. A. S. (2021). Selective separation of Sc (III) and Zr (IV) from the leaching of bauxite residue using trialkylphosphine acids, tertiary amine, tri-butyl phosphate and their mixtures. *Separation and Purification Technology, 279*, 13.

Castaldi, P., Silvetti, M., Santona, L., Enzo, S., & Melis, P. (2008). XRD, FTIR, and thermal analysis of bauxite ore-processing waste (red mud) exchanged with heavy metals. *Clays and Clay Minerals, 56*, 461–469.

Castaldi, P., Silvetti, M., Enzo, S., & Deiana, S. (2011). X-ray diffraction and thermal analysis of bauxite ore-processing waste (red mud) exchanged with arsenate and phosphate. *Clays and Clay Minerals, 59*, 189–199.

César, C., Melo, A., Simões, R., Patrícia, S., & Paz, A. (2020). A proposal for rapid grade control of gibbsitic bauxites using multivariate statistics on XRD data. *Minerals Engineering, 157*, 106539.

Chen, Z., Wang, Y., Liao, S., & Huang, Y. (2020). Grinding kinetics of waste glass powder and its composite effect as pozzolanic admixture in cement concrete. *Construction and Building Materials, 239*, 117876.

Chu, T. P. M., Nguyen, N. T., Vu, T. L., Dao, T. H., Dinh, L. C., Nguyen, H. L., Hoang, T. H., Le, T. S., & Pham, T. D. (2019). Synthesis, characterization, and modification of alumina nanoparticles for cationic dye removal. *Materials, 12*(450), 1–15.

Clark, M. W., Johnston, M., & Reichelt-Brushett, A. J. (2015). Comparison of several different neutralisations to a bauxite refinery residue: Potential effectiveness environmental ameliorants. *Applied Geochemistry, 56*, 1–10.

Dani, N., Formoso, M. L. L., Decarreau, A., & Meunier, A. (2001). Nordstrandite in bauxite derived from phonolite, lages, Santa Catarina, Brazil. *Clays and Clay Minerals, 49*, 216–226.

Dillinger, B., Batchelor, A., Katrib, J., Dodds, C., Suchicital, C., Kingman, S., & Clark, D. (2020). Microwave digestion of gibbsite and bauxite in sodium hydroxide. *Hydrometallurgy, 192*, 105257.

Dodoo, D., Ellen, G., Seguwa, E., Yawson, C., Appiah, G., Suleiman, N., & Yaya, A. (2022). Eco-efficient treatment of hazardous bauxite liquid-residue using acid-activated clays. *Cleaner Chemical Engineering, 3*, 100040.

Fabre, C., Buche, P., Rouau, X., & Mayer-laigle, C. (2020). Milling itineraries dataset for a collection of crop and wood by-products and granulometric properties of the resulting powders. *Data in Brief, 33*, 106430.

Freitas, V., Hulmann, A., Zimmer, J., Barbeiro, L., Gomes, R., Thomy, M., & Dultra, M. (2018). Soil quality and reforestation of the Brazil nut tree (Bertholletia excelsa Bonpl.) after laterite-type bauxite mining in the Brazilian Amazon forest. *Ecological Engineering, 125*, 111–118.

Giels, M., Hertel, T., Gijbels, K., Schroeyers, W., & Pontikes, Y. (2022). High performance mortars from vitrified bauxite residue; the quest for the optimal chemistry and processing conditions. *Cement and Concrete Research, 155*, 106739.

Gräfe, M., Power, G., & Klauber, C. (2011). Bauxite residue issues: III. *Alkalinity and Associated Chemistry. Hydrometallurgy, 108*, 60–79.

Habashi, F. (1997). Handbook of Extractive Metallurgy. *Volume II: Primary Metals, Secondary Metals, Light Metals*. Heidelberg, Germany: Wiley-VCH.

Hill, V. G. (1980). Proceedings, 4th International Congress for the Study of Bauxites, Alumina and Aluminum. Vol.

1, Bauxites; Vol. 2, Bauxites; Vol. 3, Alumina and Aluminum. *Clays and Clay Minerals, 28*, 70.

Jiang, Z., Quan, X., Zhao, S., Zeng, K., Chen, H., & Zhou, Y. (2021). Dealkalization and leaching behavior of Fe, Al, Ca, and Si of Red Mud by waste acid from titanium white production. *ACS Omega, 6*, 32798–32808.

Khairul, M. A., Zanganeh, J., & Moghtaderi, B. (2019). The composition, recycling and utilisation of Bayer red mud. *Resources, Conservation and Recycling, 141*, 483–498.

Kyriakogona, K., Giannopoulou, I., & Panias, D. (2017). Extraction of aluminium from Kaolin: A comparative study of hydrometallurgical processes. *Proceedings of the World Congress on Mechanical, Chemical, and Material Engineering, 133*, 2–7.

Lagauche, M., Larmier, K., Jolimaitre, E., & Barthelet, K. (2017). Thermodynamic characterization of the hydroxyl group on the γ - alumina surface by the energy distribution function. *Journal of Physical Chemistry C, 121*, 16770–167822.

Li, C., Tang, L., Jiang, J., Zhu, F., Zhou, J., & Xue, S. (2020a). Alkalinity neutralization and structure upgrade of bauxite residue waste via synergistic pyrolysis with biomass. *Journal of Environmental Sciences, 93*, 41–47.

Li, P., Yu, W., Du, Y., Lai, X., Weng, S., Pang, D., Xiong, G., Lei, Z., Zhao, S., & Yang, S. (2020b). Influence of geomorphology and leaching on the formation of Permian bauxite in northern Guizhou Province, South China. *Journal of Geochemical Exploration, 210*, 106446.

Li, H., Chai, W., Cao, Y., & Yang, S. (2022). Flotation enhancement of low-grade bauxite using oxalic acid as surface pretreatment agent. *Applied Surface Science, 577*, 151964.

Liu, R. X., & Poon, C. S. (2016). Effects of red mud on properties of self-compacting mortar. *Journal of Cleaner Production, 135*, 1170–1178.

Liu, S., Li, Q., Xie, G., Li, L., & Xiao, H. (2016). Effect of grinding time on the particle characteristics of glass powder. *Powder Technology, 295*, 133–141.

Liu, S., Zhang, J., Sun, Z., & Han, D. (2023). Effects of temperature and pressure fluctuations on exergy loss characteristics of hydrogen auto-ignition processes. *International Journal of Hydrogen Energy, 48*, 38484–38495.

Luo, J., Rao, M., Liu, M., Li, G., & Jiang, T. (2014). (2014) Extraction of Alumina from Coal-Derived Pyrite Flotation Tailing by Pre-Desilication-Bayer Process. *Light Metals, 9781118889*, 125–130.

Manjare, S. D., & Donolikar, Y. (2022). Effect of atmospheric and operational variables on dispersion of bauxite particulates at Mormugaon Port, Goa, India. *Materials Today: Proceedings, 67*, 1190–1196.

Melo, C. C. A., Angélica, R. S., & Paz, S. P. A. (2020). A proposal for rapid grade control of gibbsitic bauxites using multivariate statistics on XRD data. *Minerals Engineering, 157*, 106539.

Mohan, B., Kloss, C., Khinast, J., & Radl, S. (2014). Regimes of liquid transport through sheared beds of inertial smooth particles. *Powder Technology, 264*, 377–395.

Mondillo, N., Di, M., Kalaitzidis, S., Boni, M., Santoro, L., & Balassone, G. (2022). Petrographic and geochemical features of the B3 bauxite horizon (Cenomanian-Turonian) in the Parnassos-Ghiona area : A contribution towards the genesis of the Greek karst bauxites. *Ore Geology Reviews, 143*, 104759.

Mondillo, N., Herrington, R., & Boni, M. (2021) Bauxites. *Encyclopedia of Geology*, 694–707

Muriel, B. H., Bressan, S., Allard, T., Morin, G., Roig, J.-Y., Couëffé, R., Aertgeerts, G., Derycke, A., Ansart, C., Pinna-Jamme, R., & Gautheron, C. (2022). Reading the climate signals hidden in bauxite. *Geochimica et Cosmochimica Acta, 323*, 40–73.

Nguyen, V.D., Ngo, S.H., Nguyen, V.L., & Huynh, T.P. (2023) Incorporation of high loss-on-ignition fly ash into high-strength mortar: Influence on short-term engineering properties. *Materials Today: Proceedings*, *In Press*, 1–5. https://doi.org/10.1016/j.matpr.2023.03.531

Ostap, S. (1986). Control of silica in the Bayer Process used for alumina production. *Canadian Metallurgical Quarterly, 25*, 101–106.

Pang, D., Yu, W., Chen, Q., Du, Y., Dai, X., Deng, K., Wu, B., Deng, X., & Zhou, J. (2023) Continental weathering led to the accumulation of Early Carboniferous bauxite deposits in the SW South China Craton. *Journal of Asian Earth Sciences*, *In Press*, 1–6

Power, G., & Loh, J. (2010). Organic compounds in the processing of lateritic bauxites to alumina: Part 1: Origins and chemistry of organics in the Bayer process. *Hydrometallurgy, 105*, 1–29.

Power, G., Loh, J. S. C., & Vernon, C. (2012). Organic compounds in the processing of lateritic bauxites to alumina Part 2: Effects of organics in the Bayer process. *Hydrometallurgy, 127–128*, 125–149.

Ruys, A. (2019a) Bauxite: The principal aluminum ore. Pp. 39–47 in: *Alumina Ceramics*. Elsevier

Ruys, A. (2019b) Refining of alumina: The Bayer process. Pp. 49–70 in: *Alumina Ceramics*. Elsevier

Santini, T. C. (2015). Application of the Rietveld refinement method for quantification of mineral concentrations in bauxite residues (alumina refining tailings). *International Journal of Mineral Processing, 139*, 1–10.

Smith, P., & Power, G. (2021). High Purity Alumina-Current and Future Production. *Mineral Processing and Extractive Metallurgy Review, 13*, 747–756.

Tabereaux, A.T. & Peterson, R.D. (2014) *Aluminum Production*. P. in: *Treatise on Process Metallurgy, Volume 3: Industrial Processes*. 839–917

Valeev, D., Pankratov, D., Shoppert, A., Sokolov, A., Kasikov, A., Mikhailova, A., Salazar-concha, C., & Rodionov, I. (2021). Mechanism and kinetics of iron extraction from high silica boehmite – kaolinite bauxite by hydrochloric acid leaching. *Transactions of Nonferrous Metals Society of China, 31*, 3128–3149.

Wang, C., Lucas, R., Milward, M., & Cooper, P. R. (2021). Particle Size Effects on Abrasion, Surface Polishing and Stain Removal Efficacy in a Tooth Model System. *Biotribology, 28*, 100196.

Wu, S. Z., Chau, K. T., & Yu, T. X. (2004). Crushing and fragmentation of brittle spheres under double impact test. *Powder Technology, 143–144*, 41–55.

Wu, Y. S., Zhang, D., Li, M. C., Bi, S. W., & Yang, Y. H. (2010). Periodical attenuation of $Al(OH)_3$ particles from seed precipitation in seeded sodium aluminate solution.

Transactions of Nonferrous Metals Society of China, 20, 528–532.

Wu, Y., Zhou, K., Zhang, X., Peng, C., Jiang, Y., & Chen, W. (2022a). Aluminum separation by sulfuric acid leaching-solvent extraction from Al-bearing $LiFePO_4$/ C powder for recycling of Fe/P. *Waste Management, 144*, 303–312.

Wu, Z., Lv, H., Xie, M., Li, L., Zhao, H., & Liu, F. (2022b). Reaction behavior of quartz in gibbsite-boehmite bauxite in Bayer digestion and its effect on caustic consumption and alumina recovery. *Ceramics International, 48*, 18676–18686.

Xue, S. G., Wu, Y. J., Li, Y. W., Kong, X. F., Zhu, F., William, H., Li, X. F., & Ye, Y. Z. (2019). Industrial wastes applications for alkalinity regulation in bauxite residue: A comprehensive review. Central South University of Technology. *Journal of Central South University, 26*, 268–288.

Yadav, S.K., Banerjee, A., Jhariya, M.K., Meena, R.S., Khan, N., & Raj, A. (2022) Eco-restoration of bauxite mining: An ecological approach. P. in: *Natural Resources Conservation and Advances for Sustainability*. 173–193 pp

Zhang, J., Bai, Y., Dong, H., Wu, Q., & Ye, X. (2014). Influence of ball size distribution on grinding effect in horizontal planetary ball mill. *Advanced Powder Technology, 25*, 983–990.

Zhang, X., Huestis, P. L., Pearce, C. I., Hu, J. Z., Page, K., Anovitz, L. M., Aleksandrov, A. B., Prange, M. P., Kerisit, S., Bowden, M. E., Cui, W., Wang, Z., Jaegers, N. R., Graham, T. R., Dembowski, M., Wang, H., Liu, J., Diaye, A. T. N., Bleuel, M., … Rosso, K. M. (2018). Boehmite and Gibbsite Nanoplates for the Synthesis of Advanced Alumina Products. *ACS Applied Nano Materials, 1*, 7115–7128.

Zhang, X., Cui, W., Hu, J. Z., Wang, H., Prange, M. P., Wan, C., Jaegers, N. R., Zong, M., Zhang, H., Pearce, C. I., Li, P., Wang, Z., Clark, S. B., & Rosso, K. M. (2019). Transformation of Gibbsite to Boehmite in Caustic Aqueous Solution at Hydrothermal Conditions. *Crystal Growth Design, 19*, 5557–5567.

Zhang, J., Wang, Q., Liu, X., Zhou, G., Xu, H., & Zhu, Y. (2022). Provenance and ore-forming process of Permian lithium-rich bauxite in central Yunnan. *SW China. Ore Geology Reviews, 145*, 104862.

Zhou, J., Ma, S., Chen, Y., Ning, S., Wei, Y., & Fujita, T. (2021). Recovery of scandium from red mud by leaching with titanium white waste acid and solvent extraction with P204. *Hydrometallurgy, 204*, 105724.

Zhou, G., Wang, Y., Qi, T., Zhou, Q., Liu, G., Peng, Z., & Li, X. (2023). Chemical Engineering Toward sustainable green alumina production : A critical review on process discharge reduction from gibbsitic bauxite and large-scale applications of red mud. *Journal of Environmental Chemical Engineering, 11*, 109433.

Zhu, X., Niu, Z., Li, W., Zhao, H., & Tang, Q. (2020). A novel process for recovery of aluminum, iron, vanadium, scandium, titanium and silicon from red mud. *Journal of Environmental Chemical Engineering, 8*, 103528.

https://doi.org/10.1007/s42860-023-00264-2 Published online by Cambridge University Press